[EA]Refrac Candidate Selection Considering Natural Fracture Orientation in the Near-Fault Damage Zone*

Travis Ramsay[1], Luisalic Hernandez[1], Jennifer Li[1], and Meftun Erdogan[1]

Search and Discovery Article #42463 (2019)**
Posted October 14, 2019

*Adapted from extended abstract prepared in conjunction with oral presentation given at 2019 AAPG Annual Convention and Exhibition, San Antonio, Texas, May 19-22, 2019
 DOI:10.1306/42463Ramsay2019

[1]Halliburton, Houston, TX (Travis.Ramsay@halliburton.com)

Abstract

A large degree of uncertainty in the characterization of natural fracture density and orientation tends to exist in the overall management of unconventional assets. As a result of this uncertainty, the understanding and application of natural fracture network characterization in reservoir management has tended to be limited and often contradictory between practitioners. As a corollary, this uncertainty extends to refrac candidate selection. In the case of natural fracture plane parallelism with respect to the fault damage zone, the stress field is anticipated to simultaneously drive the formation of faults and fractures within a near concurrent time period. Alternatively, fracture plane orthogonality relative to the fault damage zone manifests away from the strongly non-proportional plastic loading zone after the re-orientation of the stress-field post-faulting. As a result, value exists in evaluating the natural fracture network considering well placement and subsurface mechanical constraints. An integrated Eagle Ford case study is shown which leverages a fault likelihood attribute and petro-elastic modeling (PEM). The fault likelihood attribute is used to spatially characterize natural fractures considering the existence of sufficient correlation between faulting and natural fracture formation. The PEM is embedded in a reservoir simulator and is used to combine dry rock elastic properties with the dynamic determination of changes in saturation. In an integrated workflow, these combined methods support the model-driven time-dependent analysis of refrac candidates linking geophysics to reservoir simulation. Typically, the simulated pressure description alone is insufficient to properly characterize refrac candidates due to the diffusive behavior of pressure. Instead, a novel dimensionless analysis of spatio-temporal saturated elastic properties is used which is more discrete and allows the fine scale characterization. The combination of fault likelihood and PEM in an integrated multidisciplinary analysis exploit geophysics in static and dynamic reservoir models to preserve the subsurface description between seismic attributes and flow simulation.

Introduction

The productivity of unconventional reservoirs has largely been focused on improving conductivity in induced fractures as well as optimizing well and stage spacing in the asset. This is, however, evaluated in the absence of a firm understanding of natural fracture systems in the subsurface which interact with induced fractures to stimulate flow through complex conduits. Previous work of Aguilera (2008) has established the value of characterizing the orientation, location, and concentration of a natural fracture system as construed by the paleo-stress environment

in order to optimize reservoir productivity. This is not to say that natural fractures are always applicable in proper characterization as these fracture types may be construed as some variant of open to healed, thus applicability is debatable (Bahrami et al. 2012; Moradian et al. 2016; Walton and McLennan 2013). Be that as it may, typical assertions for this omission are often centered on operating expenses and schedules as well as diminished technology but another consideration is that the impact of natural fracture systems in the complex fracture network is not well understood or properly characterized. This will often lead to substitutions in developed reservoir models that lead to adequate history matching but can also often be described as cryptic and lacking adequate geologic context.

This work proposes the use of a seismically derived fault likelihood attribute (Hale 2013) to spatially constrain the natural fracture network (NFN) (Lomask et al. 2017; Ramsay et al. 2017; Ramsay et al. 2018). The use of such a method enables the spatial characterization of natural fractures in a model as fractures cannot be imaged in many cases using seismic techniques but are dependent on image logs at well locations. The applicability of the enforced spatial constraint is, of course, contingent on sufficient correlation between fault location and fracture density; however, this is taken into consideration in this work through the examined post-faulting fracturing in the presence of a re-oriented stress field. It is noted that a numerical fracture model is not used in this study; instead statically re-oriented natural fracture distributions are implemented relative to the extracted fault locations and orientations. These extracted faults are the result of the fault likelihood analysis and are leveraged in a statistical analysis of fault geometries to improve the NFN. Subsequently, the NFN is utilized as a constraint to the distribution of petrophysical properties in an earth model that is built on an unstructured grid and then used in a reservoir simulator to numerical model production. Embedded in the reservoir simulator is a PEM which concurrently computes saturated dynamic elastic properties that are governed by production-induced changes. Although some would aver that the changes in saturated elastic properties are of less significance on the time scale of unconventional asset production, a dimensionless analysis of saturated elastic properties illustrates the value of this data type in the context of this solution.

Theory

The workflow under consideration is multidisciplinary in nature given that it involves data, processes, and analyses from geophysicists, geologists, and reservoir engineers to enable better decision making across the asset team for refrac candidate selection. The executed workflow is demonstrated in Figure 1 showing:

- Extraction of fault surfaces
- Statistical evaluation of fault surfaces for spatial orientation and density
- Development of an earth model
    - Constrained by the distribution of its properties with P-impedance and simulated natural fracture
- Development of an unstructured 3D geocellular array
    - Including both natural and induced fractures
- Flow simulation with an embedded PEM

Fault-likelihood, also referred to as fault-oriented semblance (Hale 2013), defines the process by which the detection of attributes in seismic data is achieved in a continuous manner that is representative of more “fault-like” behavior and is expressible in the unstructured geocellular array. Due to sufficiently observed correlation between the determined fault and natural fracture locations (Haneberg 1995; Hale 2013; Ramsay et al. 2017; Ramsay et al. 2018), the earth model was developed by constraining the distribution of petrophysical properties with P-impedance and the simulated NFN. Prior works (Hutchinson 1983; Haneberg 1995; Shipton and Cowie 2003; Lomask et al. 2017; Ramsay et al. 2018) have highlighted that natural fractures manifest proximal to faults, especially by the fault tip according to Cooke 1997.

The NFN in these simulation models were characterized as explicitly open, thus considered conduits for flow. This assumption aligns with prior work which suggests natural fractures can enable increased productivity in unconventional plays (Bahrami et al. 2012; Moradian et al. 2016); however, it is noted that others have argued that natural fractures have limited effect or obfuscate communication within otherwise sufficiently conductive zones (Walton and McLennan 2013). The former argue that natural fractures may reduce productivity as a result of cementation or extensive communication between wells. In this study, productivity is assumed to increase as the open natural fractures have simply maximized the surface area of the matrix to the completion without being inhibited by equilibrating pressure due to neighboring production wells.

The flow simulation was performed on an unstructured 3D geocellular array that encompassed natural and hydraulic fractures included as discretized properties. This particular reservoir flow simulator includes an embedded PEM (Landmark, 2019) which is typically used to reconcile simulated production in integrated 4D seismic to simulation solutions (Emerick et al. 2007; Li et al. 2008; Milicevic and Ferguson 2010; Ramsay et al. 2017; Ramsay et al. 2018); but here is leveraged to infer the seismic response in the simulation model in order to appropriately evaluate refrac candidates. While the reservoir simulator includes two PEMs, the particular embedded PEM that was incorporated into this study is the Batzle and Wang (1992) method. The Batzle and Wang (1992) method works by estimating saturated elastic rock properties based on thermodynamic correlations and leverages the available fluid description that has been incorporated into the reservoir simulator (Landmark, 2019). The main objective in the computation is the calculation of time-dependent P-impedance in the reservoir simulator, which is expressed as:

$$Z_p = \rho_{sat} V_p \qquad (1)$$

The determination of the time-dependent saturated rock density is construed by proportionately weighting the dry rock matrix density and the component fluid densities. This is described according to:

$$\rho_{sat} = \rho_{matrix}(1-\varphi) + \rho_w S_w \varphi + \rho_{hc}(1-Sw)\varphi \qquad (2)$$

Next, the time-dependent compressional velocity is computed by first employing the Gassmann equation, expressed according to a rearranged form analogous to Mavko et al. 2009:

$$K_{sat} = \frac{\varphi\left(\frac{1}{K_0} - \frac{1}{K_{fl}}\right) + \frac{1}{K_0} - \frac{1}{K_{dry}}}{\left(\frac{\varphi}{K_{dry}}\right)\left(\frac{1}{K_0} - \frac{1}{K_{fl}}\right) + \left(\frac{1}{K_0}\right)\left(\frac{1}{K_0} - \frac{1}{K_{dry}}\right)} \quad (3)$$

The saturated shear modulus, which is equivalent to the dry rock shear modulus (μ_{dry}), is then combined with the K_{sat} and ρ_{sat} terms in order to compute the time-dependent compressional and shear velocity:

$$V_p = \sqrt{\frac{K_{sat} + \frac{4}{3}\mu_{sat}}{\rho_{sat}}} \quad (4)$$

$$V_s = \sqrt{\frac{\mu_{sat}}{\rho_{sat}}} \quad (5)$$

It is well understood from literature that natural fractures are formed based on the following characteristics: cementation, energy release rate, fracture energy, proximal fault slip, lithology, grain size distribution, and temperature (Schmidt 1977; Cleary 1978; Yin and Rogers 1995; Fitzenz and Miller 2004; Eseme et al. 2007; Jin et al. 2010). This study builds on the findings of Yin and Rogers (1995) which describes the rotation of the stress field during tectonic faulting processes. Subsequently, substantial far-field and local re-orientation of the principal horizontal stress in the proximity of tectonic faulting events were averred by Fitzenz and Miller (2004). The objective of this work is to investigate refrac candidate selection in the presence of locally varying natural fracture alignment with respect to oriented fault tip under parametric considerations. The investigation takes place considering post-faulting natural fracture placement without determining post-faulting rotation angle (Yin and Rogers 1995). The resulting imposed rotations are therefore a function of energy release rate, fracture energy, principal horizontal stress, and time assuming behavior described according to linear elastic fracture mechanics. It is postulated here that parallel natural fracture and fault orientation manifests as a result of expedited expression of energy release rate in the process zone; while off-axis angles of rotation distinguishing the orientation of natural fractures to faults represent slower post-fault expressions of fracture energy.

Results and Discussion

The fault likelihood attribute was used to extract fault surfaces that are characterized by orientation and density. Subsequently, these results were propagated to an unstructured 3D geocellular array which allowed them to be used as a constraint to NFN simulation. This work also assumes the same fault zone description as Ramsay et al. 2018, which describes the fault zone as a zone of messy inelasticity similar to the process zone in linear elastic fracture mechanics at the micro-scale.

Three cases of natural fracture orientation relative to fault axis were evaluated through selected NFN simulation scenarios and are shown in Figure 2. The description of the well and geometric description of induced fractures are shown in Table 1.

This particular Eagle Ford project represents a saturated oil zone with a generic Corey-type relative permeability description. A Batzle and Wang (1992) PEM method was used to estimate P-impedance and other elastic properties dynamically based on simulated changes in pressure and saturation. The requisite dry rock bulk modulus, shear modulus, and matrix density were assigned to the unstructured 3D geocellular grid through categorical classification of existing grid array properties that were incorporated in the petrophysical model. The referred description is analogous to Ramsay et al. (2017) and Ramsay et al. (2018); thus, the interested reader may review further.

Over the 1,000 days of simulated production, variations in pressure communication between wells and adjacent stages manifests as a result of the interaction between well conditions and the complex fracture network. Illustrated in Figure 3 are the pressure profiles at 486 days and 974 days of simulated production, respectively. The figures show that marginal communication between wells exists at 486 days but becomes more extensive by 974 days. While some estimation can be made about refrac candidate selection using the pressure profiles, there are limitations to interpretation due to the diffusive behavior of pressure in the assumed potentially productive zones. The same can be said of analyzing dimensional representations of P-impedance which tend to obfuscate changes in P-impedance due to production over time from unconventional formations due to their magnitude. Thus, further refrac candidate analysis is suggested which is based on dimensionless saturated elastic rock properties to address discernibility characteristics of the potentially productive zones.

The dimensionless saturated elastic rock space specifically involves representing dynamic P-impedance, computed by the reservoir simulator, the normalized difference of P-impedance between two disparate simulated times (Ramsay and Yarus 2016; Ramsay et al. 2017). The normalization scheme that was employed is described as:

$$Z_{p,1:2} = 10^{0.1\left(\frac{Z_{p,1} - Z_{p,2}}{Z_{p,1}}\right)} - 0.5 \qquad (6)$$

The exponent in this expression directly represents the normalization but the additional scaling is enforced to enhance analysis and interpretive capabilities during visualization. In Equation 6, $Z_{p,1}$ is the simulator-derived P-impedance at time t_1 and $Z_{p,2}$ is the simulator-derived P-impedance at time t_2, such that $t_1 < t_2$. Results from the dimensionless representation are shown in Figure 4 and indicate that the dimensionless representation of P-impedance enables:

- Detectability of higher frequency spatio-temporal changes
- Amplification of changes in P-impedance compared to background properties
- Discretized saturated rock properties that are less diffuse

In the context of Equation 6, $Z_{p,1}$ is computed at the 0^{th} time-step while $Z_{p,2}$ is computed at 486 simulated days and 974 simulated days, respectively. In the vicinity of the stimulated reservoir volume, lower dimensionless P-impedance suggests unexploited (bypass) oil and gas; whereas higher dimensionless P-impedance suggests depleted hydrocarbon fluid volume.

The simulated P-impedance reduces between the simulated 486 days and 974 days due to production which would not have been evident if the P-impedance remained dimensional. The least productive scenario is Case 3, where NFN and induced fracture interaction is a maximum. This is in contrast to Case 1 where the NFN and induced fractures interaction is minimal. Figure 5 illustrates the production profiles from each simulation case. It is clear that commensurate with the aforementioned NFN-induced fracture interaction description that Case 1 demonstrates the most productive scenario and Case 3 demonstrates the least productive scenario, as a corollary. Due to the impact of natural fracture orientation on production it is suggested that the orientation of these natural fractures also be considered in refrac design; especially since the effects of stress shadowing need to be considered (Nagel and Sanchez-Nagel 2011; Sobhaniaragh et al. 2018).

The production plateau is established for both oil and gas during approximate 60% of the first year of simulated production. In each case, a combination of the production profiles and the dimensionless P-impedance can be used to evaluate refrac candidate opportunities. While it is acknowledged that opportunities for refrac exist outside of the 486 day and 974 day timelines, the evaluation only focuses on these timelines for illustrative purposes. Areas demonstrating greater dimensionless P-impedance for each case at the simulated 486 days and 974 days illustrate opportunities for refrac candidate selection. For Case 1, Figure 4a shows induced fractured zones that interact directly with the matrix and with natural fractures leading to reductions in dimensionless P-impedance due to a combination of oil production and gas coming out of solution as well as the effect of the pressure gradient. Recall that P-impedance represents the product of saturated density with compressional velocity. Within each well the comingled natural and induced fractures interact leaving few under-stimulated zones. As the simulation progresses, it is clear in Figure 4d that the zones with minimal changes in dimensionless P-impedance remain in this state as changes in saturated density near the induced fracture continue to illustrate the manifestation of gas. In Case 2, Figure 4b shows additional refrac opportunities between fracture stages according to the map of dimensionless P-impedance at 486 simulated days. Inter-well communication between the complex fracture system is minimal between the toe and heel of the well and zones between fracture stages with larger amounts of unchanged dimensionless P-impedance remain as well. As the simulation is advanced to 976 days, in Figure 4e natural fracture communication can be seen as the applied pressure gradient affects the inter-well and between fracture stages in individual wells. A similar result to Case 2 occurs in Case 3 and is illustrated in Figure 4c; however, with the change in natural fracture orientation existing such that they are aligned between the wells, inter-well communication is established earlier in Case 3. By the 976 simulated days, the communication between the wells through the natural fractures is more extensive, as illustrated in Figure 4f, compared to the similar time examined for Case 2. Given the existence of unchanged dimensionless P-impedance in the stimulated reservoir volume, Case 2 and 3 respectively illustrate opportunities where refrac candidates exist according to the simulated dimensionless P-impedance and the decline in production. Between the two cases; however, a preferred refrac candidate selection exists in Case 2 due to the lack of communication between wells through the complex fracture network. This determination is in juxtaposition to Case 3 where the fracture experiences greater amounts of communication. Thus, although Case 3 was the least productive, Case 2 represents the greater refrac candidate opportunity during the observed timelines as the pressure field between the wells does not equilibrate, as extensively, due to the early onset complex fracture interaction.

Conclusions

The results of this study demonstrate the combination of fault likelihood attribute, natural fracture network conditioning, petrophysical property modeling, and dynamic simulation in an integrated solution focused on refrac candidate selection. The nominal spacing of wells and fracture spacing were used as control while a parametric evaluation of post-faulting stress orientation expressed as azimuthal variation in NFN relative

to interpreted faults, and to the wells as a corollary, were examined. Even though the natural fractures were assumed to possess high conductivity to facilitate this investigation, greater attention should be placed on the inclusion and orientation of NFN when evaluating refrac candidates. The broad distribution of high conductivity natural fractures in reality is not anticipated as over time, varying amounts of cementation would otherwise impede flow; but localized high conductivity zones are proposed to exist. The existence of varied characterizations of conductivity is evident in the argument for sources of improved productivity (Bahrami et al. 2012; Moradian et al. 2016) compared to arguments against it (Walton and McLennan 2013). The results of the study demonstrated how a dimensionless PEM may be incorporated into refrac candidate selection. Areas of low dimensionless P-impedance indicated little or reduced stimulated reservoir volume which could potentially be further exploited by refrac. The results showed that even where productivity was at a minimum compared to the other evaluated scenarios that the petroelastic response and the inter-well communication through the complex fracture network highlighted the areas where a refrac could potentially be more successful.

References Cited

Aguilera, R., 2008, Effect of Fracture Compressibility on Gas-in-Place Calculations of Stress-Sensitive Naturally Fractured Reservoirs: SPE Reservoir Evaluation and Engineering, SPE-100451-PA, v. 11/2, p. 307-310. doi.org/10.2118/100451-PA

Bahrami, H., R. Rezaee, and M. Hossain, 2012, Characterizing Natural Fractures Productivity in Tight Gas Reservoirs: Journal of Petroleum Exploration and Production Technology, v. 2/2, p. 107-115.

Batzle, M., and Z. Wang, 1992, Seismic Properties of Pore Fluids: Geophysics, v. 57/11, p. 1396-1408.

Cleary, M., 1978, Some Deformation and Fracture Characteristics of Oil Shale: 19th U.S. Symposium on Rock Mechanics, Reno, Nevada, USA, 1-3 May, ARMA-78-0088.

Cooke, M., 1997, Fracture Localization Along Faults with Spatially Varying Friction: Journal of Geophysical Research, v. 102/B10, p. 22,425-22,434.

Emerick, A., R. Moraes, and J. Rodrigues, 2007, Calculating Seismic Attributes Within a Reservoir Flow Simulator: Latin American & Caribbean Petroleum Engineering Conference, Buenos Aires, Argentina, 15-18 April, SPE-107001-MS. doi.org/10.2118/107001-MS

Eseme, E., J.L. Urai, B.M. Krooss, and R. Littke, 2007, Review of Mechanical Properties of Oil Shales: Implications for Exploitation and Basin Modelling: Oil Shale, v. 24/2, p. 159-174.

Fitzenz, D.D., and S.A. Miller, 2004, New Insights on Stress Rotations from a Forward Regional Model of the San Andreas Fault System Near its Big Bend in Southern California: Journal of Geophysical Research, v. 109, B08404, 17 p. doi:10.1029/2003JB002890

Hale, D., 2013, Methods to Compute Fault Images, Extract Fault Surfaces, and Estimate Fault Throws from 3D Seismic Images: Geophysics v. 78/2, p. 33-43.

Haneberg, W.C., 1995, Steady State Groundwater Flow Across Idealized Faults: Water Resources Research, v. 31/7, p. 1815-1820.

Hutchinson, J.W., 1983, Fundamentals of Phenomenological Theory of Nonlinear Fracture Mechanics: Journal of Applied Mechanics, v. 50, p. 1042-1051.

Jin, Z.-H., S.E. Johnson, and Z.Q. Fan, 2010, Subcritical Propagation and Coalescence of Oil-Filled Cracks: Getting the Oil Out of Low-Permeability Source Rocks: Geophysical Research Letters, v. 27/01. doi.org/10.1029/2009GL041576

Landmark Software and Solutions, 2019, Nexus User Manual. Houston, Texas: Landmark.

Li, H., X. Tai, and S. Aanonsen, 2008, Reservoir Description by Using a Piecewise Constant Level Set Method: Journal of Computational Mathematics, v. 26/3, p. 365-377.

Lomask, J., L. Hernandez, V. Liceras, A. Kumar, and A. Khadeeva, 2017, A Seismic to Simulation Unconventional Workflow Using Automated Fault-Detection Attributes: Interpretation, v. 5/3, p. SJ41-SJ48. doi.org/10.1190/INT-2016-0148.1

Mavko, G., T. Mukerji, and J. Dvorking, 2009, The Rock Physics Handbook, Second Edition – Tools for Seismic Analysis of Porous Media: Cambridge University Press, New York, New York, USA. doi.org/10.1017/CBO9780511626753

Milicevic, V., and R. Ferguson, 2010, Numerical Fluid Flow Modeling and its Seismic Response in Time-Lapse: Geo-Canada 2010, Calgary, Alberta, Canada, 10-13 May.

Moradian, Z., A. Fathi, and B. Evans, 2016, Shear Reactivation of Natural Fractures in Hydraulic Fracturing: 50th US Rock Mechanics/Geomechanics Symposium, Houston, Texas, USA, 26-29 June, ARMA-2016-829.

Nagel, N., and M. Sanchez-Nagel, 2011, Stress Shadowing and Microseismic Events: A Numerical Evaluation: SPE Annual Technical Conference and Exhibition, Denver, Colorado, U.S.A., 30 October-2 November.

Ramsay, T, and J. Yarus, 2016, Simulation Enabled Petro-Elastic Modeling Methods in a Fractured Low Permeability Reservoir: Third EAGE Integrated Reservoir Modeling Conference, Kuala Lumpur, Malaysia, 5-7 December. doi:10.3997/2214-4609.201602406

Ramsay, T., L. Hernandez, J. Lomask, and A. Sullivan, 2017, Improved Fracture Productivity Prediction Using Enhanced Seismic Attributes: Abu Dhabi International Petroleum Exhibition & Conference, Abu Dhabi, UAE, 13-16 November, SPE-188757-MS. doi.org/10.2118/188757-MS

Ramsay, T., L. Hernandez, J. Li, and M. Erdogan, 2018, Fracture Productivity Prediction Considering Natural Fracture Formation Proximal to Fault Damage Zone: Unconventional Resources Technology Conference, Houston, Texas, USA, 23-25 June, URTeC: 2900588.

Schmidt, R.A., 1977, Fracture Mechanics of Oil Shale – Unconfined Fracture Toughness, Stress Corrosion Cracking and Tension Test Results: 18th U.S. Symposium on Rock Mechanics, Keystone, Colorado, USA 22-24-June, ARMA-77-082.

Shipton, Z.K., and P.A. Cowie, 2003, A Conceptual Model for the Origin of Fault Damage Zone Structures in High Porosity Sandstone: Journal of Structural Geology, v. 25/3, p. 333-344.

Sobhaniaragh, B., M. Haddad, W.J. Mansur, and F.C. Peters, 2018, Computational Modelling of Multi-State Hydraulic Fractures Under Stress Shadowing and Intersecting with Pre-Existing Natural Fractures: Acta Mechanica, v. 230/1, p. 1037-1059. doi.org/10.1007/s00707-018-2335-8

Walton, I., and J. McLennan, 2013, The Role of Natural Fractures in Shale Gas Production, *in* A.P. Bunger, J. McLennan, and R. Jeffrey (eds), Effective and Sustainable Hydraulic Fracturing: IntechOpen, London, UK. doi:10.5772/56404

Yin, Z., and G. Rogers, 1995, Rotation of the Principal Stress Directions Due to Earthquake Faulting and its Seismological Implications: Bulletin of the Seismological Society of America, v. 85/5, p. 1513-1517.

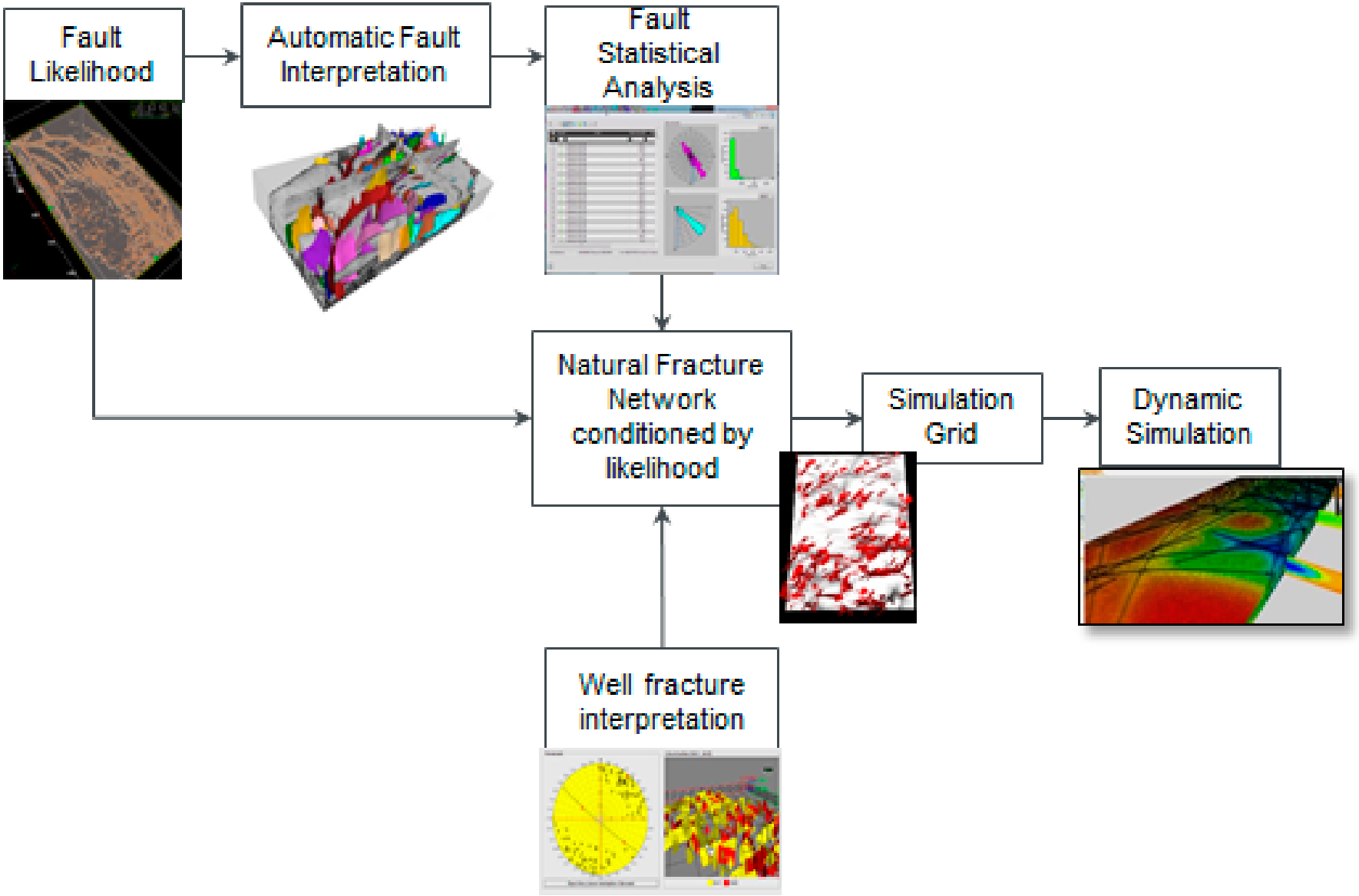

Figure 1. Multidisciplinary workflow highlighting integrated seismic attribute development through simulation.

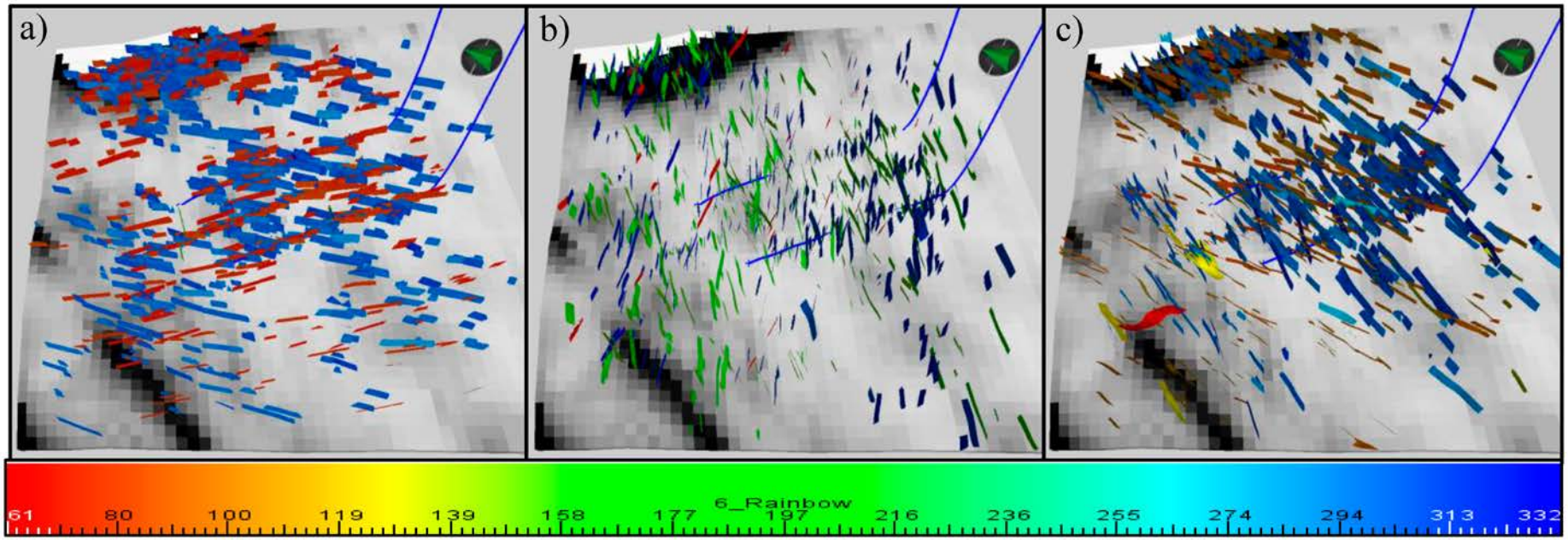

Figure 2. 3D natural fracture network for scenarios describing: a) 0˚ , b) 90˚ and 45˚, respectively, relative to the orientation of the fault likelihood derived faults (colored by azimuthal direction) including the fault likelihood attribute in the background.

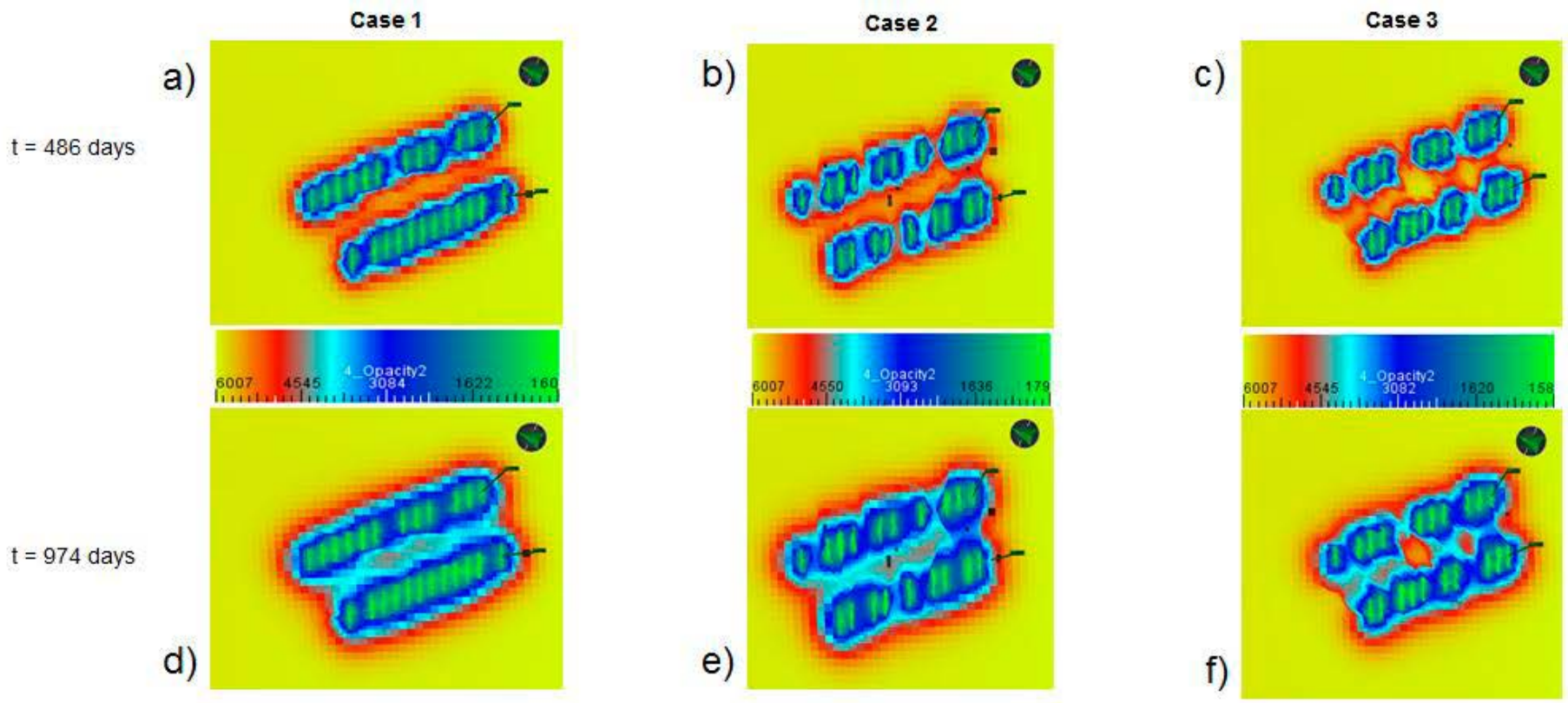

Figure 3. Pressure field for Case 1 – a) 486 days and d) 974 days; Case 2 – b) 486 days and e) 974 days; and Case 3 – c) 486 days and f) 974 days.

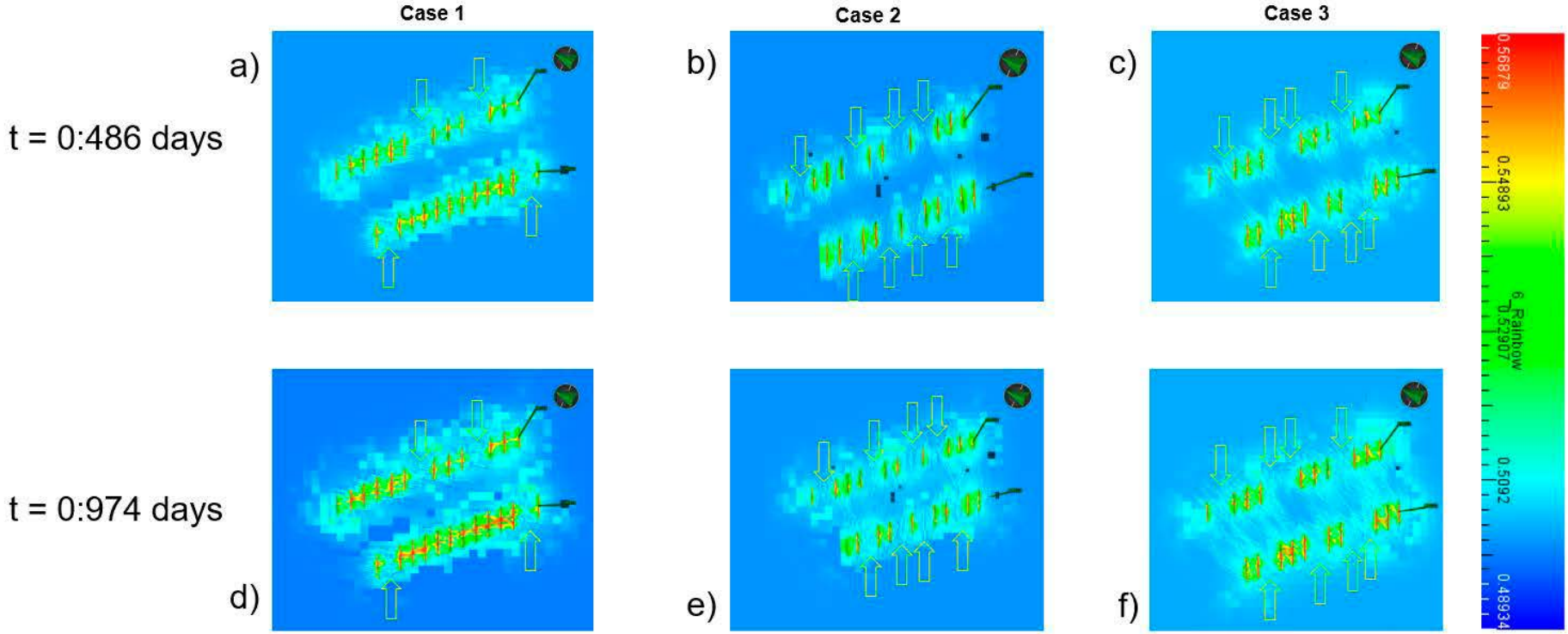

Figure 4. Dimensionless P-impedance computed between zeroth time-step and: Case 1 a) 486 days, d) 974 days; Case 2 b) 486 days, e) 974 days; and Case 3 c) 486 days and f) 974 days. The yellow arrows indicate the low change dimensionless P-impedance zones.

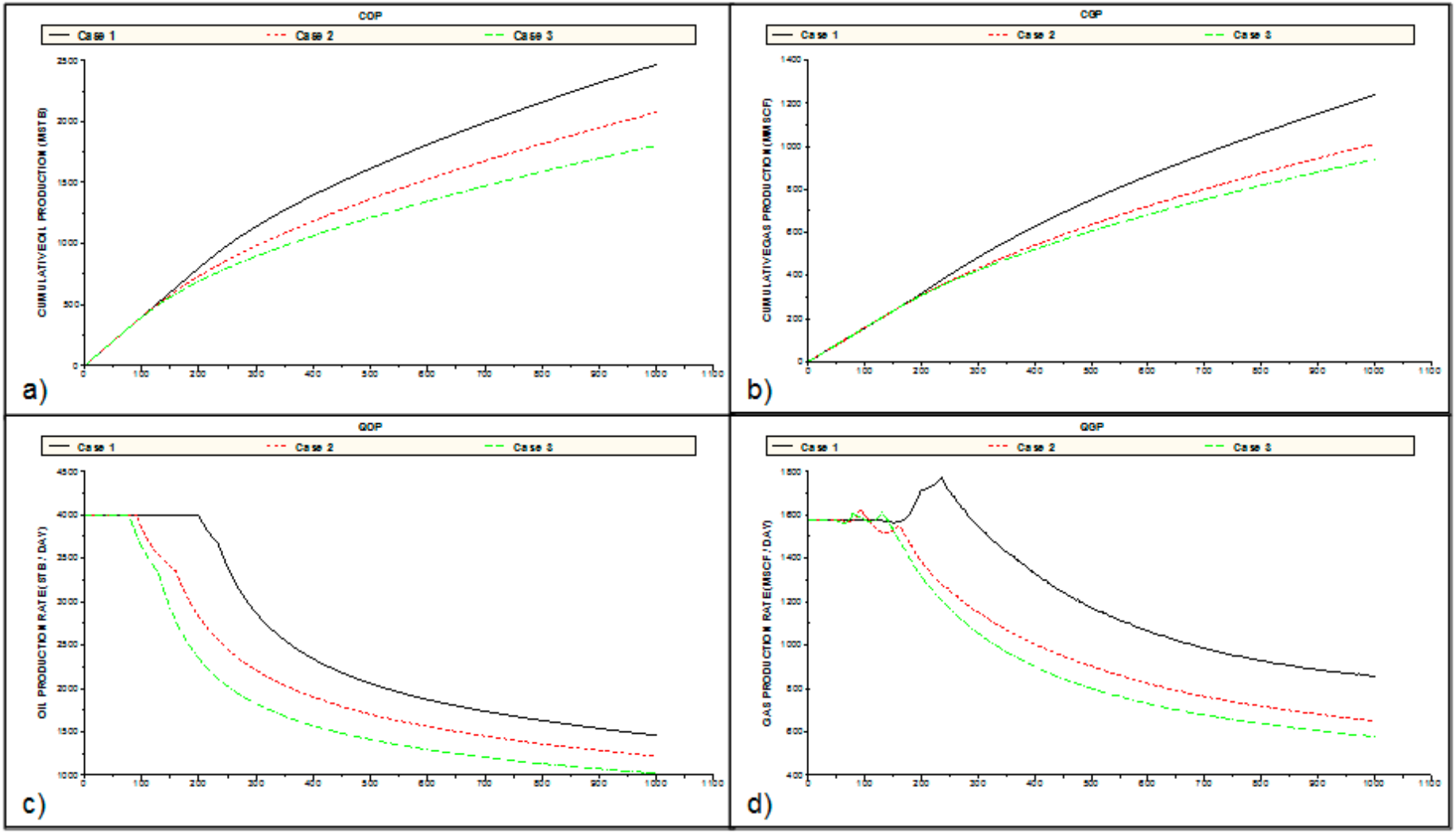

Figure 5. Simulation production profiles for: a) cumulative oil production, b) cumulative gas production, c) oil production rate, and d) gas production rate for the two wells in the project.

Well Name	Description		
	Number of Induced Fractures	Fracture Half-Length (ft)	Fracture Spacing (ft)
Well1	14	350	450
Well2	14	400	400

Table 1. Well summary description.